Ta-ITO Coated Titanium Bipolar Plates for Proton Exchange Membrane Water Electrolyzers

Journal of The Electrochemical Society, 2022 **169** 034504

Ta-ITO Coated Titanium Bipolar Plates for Proton Exchange Membrane Water Electrolyzers

Sigrid Lædre,[1,2,z] Lucia Mendizabal,[3] Ole Edvard Kongstein,[5,†] Anders Oedegaard,[2] Håvard Karoliussen,[4] and Frode Seland[1,*]

[1]*Department of Materials Science and Engineering, Norwegian University of Science and Technology, Trondheim, Norway*
[2]*Department of Sustainable Energy Technology, SINTEF Industry, Trondheim, Norway*
[3]*Physics of Surfaces and Materials Department, TEKNIKER, Basque Research and Technology Alliance (BRTA), Eibar, Spain*
[4]*Department of Energy and Process Engineering, Norwegian University of Science and Technology, Trondheim, Norway*
[5]*Department of Materials and Nanotechnology, SINTEF Industry, Trondheim, Norway*

A novel bi-layer coating composed of a tantalum base layer with an Indium Tin Oxide (ITO) top layer was applied to titanium substrates. Samples were polarized ex situ in a parameter study, where the pH, potential and temperature of the electrolyte was altered, as well as the polarization duration. The Interfacial Contact Resistance (ICR) after polarization showed an increase with time for the first 24 h, then stabilized at approx. 30 mΩ cm2. Minor variations were seen in the ICR after polarization at 1.4 V_{RHE} and 2.0 V_{RHE}, but after polarization at 2.5 V_{RHE} and 2.6 V_{RHE}, the ICR increased to 102 mΩ cm^2 and 503 mΩ cm^2, respectively. X-ray photoelectron spectroscopy (XPS) analysis revealed that the oxygen to metal ratio on the Tantalum- Indium Tin Oxide (Ta-ITO) coated sample surfaces increased with increasing polarization potential. The surfaces of the samples polarized at 2.5 V_{RHE} and 2.6 V_{RHE} showed lower concentrations of oxygen vacancies, an increase in hydroxides and a decrease in metallic character compared to the non-coated and baseline samples. ITO proved to be a promising candidate for use as coating on BiPolar Plates (BPPs) in Proton Exchange Membrane Water Electrolyzers (PEMWEs).
 [DOI: 10.1149/1945-7111/ac56a3]

Manuscript submitted September 9, 2021; revised manuscript received January 16, 2022. Published March 4, 2022.

As the world's energy consumption grows, it is evident that the anthropogenic influence on the atmospheric greenhouse effect causes irreparable damages, and there is a strong need for increased implementation of renewable energy sources.[1–3] Hydrogen, which is one of the most abundant elements on the Earth's surface, is considered one of the most promising energy carriers for the future.[4–6] There are several methods for producing hydrogen, but today it is predominantly produced by steam reforming of natural gas (methane) or gasification of coal and oil.[3,4] These methods are cost effective, but result in the production of CO_2, impeding the transition to renewable energy sources. Water electrolysis powered by renewable energy is a more environmentally friendly method for producing hydrogen, as it does not depend on fossil fuels, nor does it result in greenhouse gas emissions. Alkaline water electrolyzers dominate the market today[2,4] with their relatively cheap components, long lifetime and low maintenance costs. Despite the advantages to the alkaline electrolyzer, it is associated with a low partial load range, limited current density and low operating pressures.[4]

Several of the drawbacks associated with the alkaline electrolyzer were overcome when the first Proton Exchange Membrane Water Electrolyzer (PEMWE) was developed by General Electric in the 1960s.[7] With a thin (20–300 μm) polymer electrolyte membrane (e.g. Nafion®, fumapem®), this electrolyzer combines high proton conductivity, low gas crossover, compact system design and high pressure operation.[4] The PEMWE is considered an interesting alternative to the alkaline water electrolyzer,[8,9] as it can operate under higher current densities and work under a wide range of power inputs.[4] Another advantage over the alkaline electrolyzer, is the lack of liquid caustic electrolyte, making the PEMWE both safer and more reliable. The PEMWE can operate dynamically, including a load following mode,[10] which make it very attractive in energy capture and storage systems where the electrical energy is obtained from e.g. wind power.

The Bipolar Plates (BPPs) are essential components in a PEMWE stack,[6] and their tasks are to separate single cells in a stack, distribute water and produced gases within the electrolyzer and conduct heat and current between single cells in a stack.[4] In addition to being electrically conductive, the BPP must have high corrosion resistance, be easy to manufacture, possess high shock durability and high mechanical strength.[6] These demands have limited the material selection for BPPs, making it an expensive part of the PEMWE.[4,10] Carmo et al.[4] estimated that the separator plates and current collectors are responsible for 48% of the total stack cost. If this is the case, the cost reduction of a PEMWE stack is very much dependent on the development of new and better BPP solutions. Compared to e.g. PEM fuel cells (PEMFC), the conditions inside a PEMWE are far more challenging for the BPP. The cell voltage and anode electrode potential in a PEMWE can under some circumstances reach 2.0 V, which limits the material selection significantly.

With its low initial resistivity, high initial thermal conductivity, low permeability and excellent strength,[4] titanium is a good candidate for BPPs in PEMWE. However, titanium is prone to degradation at the anode side of the electrolyzer, and the development of oxides on its surface causes an increase of the Interfacial Contact Resistance (ICR). Coated titanium has been studied as a BPP material for electrolyzers and regenerative fuel cells and is used in commercial electrolyzers today.[4,6,11–16] Lin et al.[13] investigated the corrosion behavior of titanium coated with (Ti, Zr)N, with the objective of using it as bipolar plate material in regenerative fuel cells. Zhang et al.[14] worked with a silver-containing coating for titanium, Ti-Ag, where they tested the corrosion properties, interfacial conductivity and surface energy. Zhang et al.[15] coated titanium with honeycomb-like Ti-Ag-N nanocomposite by use of a DSHP-700 arc ion plating system. X-ray diffraction (XRD), Scanning Electron Microscopy (SEM) and ICR were used to characterize the coating, and the samples were put through both potentiostatic and potentiodynamic polarizations. Other materials and coatings have also been investigated as possible BPP solutions in electrolyzers.[16–20] For example, Langemann et al.[17] and Gago et al.[18] tested coatings for stainless steel BPPs in PEMWE. Hansen et al.[20] investigated highly alloyed stainless steel as BPP material for

*Electrochemical Society Member.
†Deceased.
zE-mail: Sigrid.ladre@sintef.no

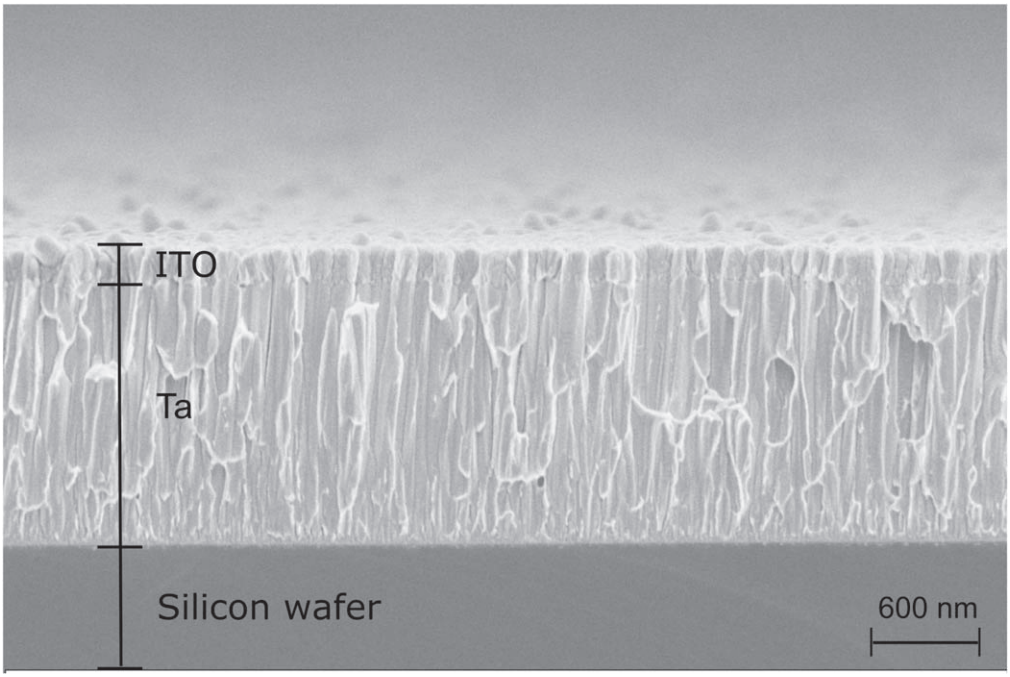

Figure 1. Cross section of a silicon wafer coated with Ta-ITO.

PEM water electrolyzers. They recommended the use of austenitic steel containing 20% nickel, 20% chromium, 3%–5% molybdenum, 0.5%–2% copper, 30%–50% iron and maximum 9% other elements. Rojas et al.[21] investigated stainless steel substrates with various chromium- and titanium nitrides, and the Ti/TiN multilayer coating proved to be the best candidate with current densities below 500 μA cm^{-2} at 2 V_{SHE} and ICR below 9.9 mΩ cm^2 after polarization.

Tantalum and tantalum oxides have been used for various applications in the past.[22–30] Due to tantalums biocompatibility, ductility and excellent corrosion resistance, it has been investigated for use in in-vivo applications.[25,27,30] Tantalum oxide's (Ta_2O_5) high dielectric constant, high refractive index, low optical absorption coefficient and high chemical stability has made it attractive for use in memory devices, coatings for photographic lenses, electrochromic devices, switchable mirror foil film, photocatalysis.[26,29] Wang et al.[31] and Alishahi et al.[32] both deposited a TaN/Ta coating on stainless plates plates for use in PEMFCs, and found good corrosion resistance. Wang et al. measured the ICR prior to polarization to 9.03 mΩ cm^2, while Alishahi et al. found it to be 12 mΩ cm^2.

Indium Tin Oxide (ITO) is a tin-doped indium oxide (In_2O_3:Sn) and an n-type semiconductor which exhibits high optical transmittance in the visible region, high electrical conductivity, surface uniformity and process compatibility.[33,34] These properties have led to the use of ITO films as transparent electrodes in e.g. flat panel displays and solar cells, surface heaters for automobile windows, camera lenses and mirrors.[34] ITO films have been deposited by vacuum evaporation,[35] spray pyrolysis,[36] Chemical Vapor Deposition (CVD),[37] sol-gel process,[38] Direct Current magnetron sputtering (DC)[39] and Radio Frequency (RF)[40] magnetron sputtering. These studies have shown the great importance of deposition technique and process parameters on microstructural, optical and electrical properties of ITO films.[33] For example, ITO films exhibit resistivity values ranging from $1{\cdot}10^{-4}$ Ω cm up to $1{\cdot}10^{-2}$ Ω cm[41,42] dependent upon growing characteristics. Magnetron sputtering is considered as the state-of-the-art ITO industrial production method in terms of ITO opto-electronic properties, process control and reproducibility.[43]

The pH experienced by a BPP inside an operating electrolyzer is difficult to measure, but there are studies that try to determine how the pH develops over time inside a PEMWE. Langemann et al.[17] measured the pH on both the anode and cathode side during operation in a PEMWE, where the BPPs had been coated with noble metals to avoid corrosion. Over a time span of 50 h, the pH values of the inlet water were found to decrease from 5.6 to 3.5 on the anodic side and from 5.6 to 4.7 on the cathodic side of the water electrolyzer.

In this work a novel corrosion-resistant and electrically conductive bi-layer coating made to improve the performance of titanium BPPs in PEMWE is presented. The bi-layer coating is composed of a tantalum layer (Ta) deposited by High Power Pulsed Magnetron Sputtering (HPPMS) followed by a successive deposition of a thin ITO layer by pulsed DC Magnetron Sputtering (pDCMS). HPPMS technique is a variation of conventional DC magnetron sputtering with much higher ionization degree of sputtered particles due to the application of high peak power short pulses with low frequency and duty cycle.[44] The increased ionization obtained by HPPMS has been utilized in this study to grow well-adhered, high density and low defect Ta layer.[45] The deposition of a thin ITO film on top of the Ta layer is intended to prevent the growth of non-conductive tantalum oxides at the anode during high voltage PEMWE operation. In addition, ITO exhibits high electrical conductivity and good corrosion resistance making it a good coating for BPPs in PEMWE. The purpose of this work was to study Ta-ITO coated titanium under conditions similar to the ones inside an operating PEMWE, with the objective of using the coating on both BPPs and sinters in PEMWE. The high potential and harsh conditions used for these tests separate this study from previous investigations of ITO for other purposes.

Experimental

Coatings and substrates.—Titanium gr. 2 coupons (3.5 × 3.5 cm) were used as substrate materials for the Ta-ITO coating in this study. A closed field unbalanced magnetron sputtering (CFUBMS) system equipped with two rectangular magnetrons (500 × 125 mm) were used for the deposition of both tantalum and ITO layers. The substrates were placed in a double rotational planetary substrate holder (8 rpm) at 120 mm from the magnetrons. The bi-layer Ta-ITO coatings were deposited by successive

sputtering of a metallic Ta target and a ceramic ITO (In_2O_3: SnO_2, 90:10 wt. %) target by HPPMS and pDCMS, respectively.

The titanium substrates were etched for 1 h in 25% HCl prior to introduction into the sputtering chamber to remove the native oxide of Ti samples. Once into the chamber, the samples were pre-heated to 250 °C and sputter etched in an Ar+H_2 mixture for 10 min in prior to coating deposition. The etching was done to clean the surface, remove the oxides and enhance coating-to-substrate adhesion. The Ta film was grown by HPPMS in Ar atmosphere at 0.7 Pa and 4 kW average power. The HPPMS pulse shape was a 1500 μs pulse with a peak power of 80 kW, a peak current of 90 A, a peak voltage of 855 V and a repetition frequency of 120 Hz. Deposition time was set to 60 min and −50 V bias voltage was applied. The ITO film was reactively sputtered by pDCMS at 0.3 Pa and 1.5 kW average power. Argon and oxygen flows were maintained constant at 75 and 3 Standard Cubic Centimeters per Minute (SCCM), respectively. The pulsing frequency was 75 kHz and the duty cycle 70%. Deposition time was 10 min, and no bias was applied. The thickness of the tantalum and ITO coatings applied to the titanium substrates were 1500 and 190 nm, respectively. Figure 1 shows a cross section image of the Ta-ITO coating on top of a silicon wafer. The silicon wafer was used for this imaging, as it is easier to cut than titanium.

Polarization.—A Gamry ref 600 potentiostat was used to polarize the plates in a conventional three-electrode electrochemical cell. In order to limit and control the exposed area of the working electrode sample, it was placed in a custom-made sample holder exposing only a circular area of 6.15 cm^2 on one side. A platinum wire was used as counter electrode, and a Reversible Hydrogen Electrode (RHE) was used as a reference. The electrolyte was made by a 0.1 M Na_2SO_4 solution, where the pH was adjusted by use of H_2SO_4 and NaOH. To minimize oxygen content in the electrolyte, Nitrogen gas (5.0 N_2. Aga) was bubbled into the solution both before and during most the polarization tests.

Various operation parameters were altered in the ex situ polarization experiments performed in this study: Temperature, pH, electrode potential and duration of polarization. The parameters used during the polarization tests are presented in Table I. The baseline parameters were chosen as they were assumed to be close to the conditions normally experienced by a BPP inside an operating electrolyzer. Most of the tests performed were at a fixed potential (potentiostatic), but potentiodynamic polarization between 0 and 2.0 V_{RHE} were also carried out. This range should cover most of the potentials experienced inside an electrolyzer. In addition to the Ta-ITO coated titanium, non-coated titanium, gold coated titanium, non-coated gold and non-coated platinum were tested at the baseline conditions. Electrochemical Impedance Spectroscopy (EIS) was performed prior to each polarization test, to obtain ohmic resistances, which were used for IR compensation (85%).

Contact resistance measurements.—ICR was measured before and after each test. A schematic of the ICR setup was shown by the authors in.[46] The resistance was measured between the test plate and a Gas Diffusion Layer (GDL). Carbon GDL is not used on the anode side in an operating electrolyzer, as it would corrode, but for these ex situ tests carbon GDLs were used to obtain comparable ICR values. The test plate and GDL were placed between two gold-coated copper plates, and a current of 2.0 A (Xantex, XDL 56–4 DC power supply) was passed through the system. The pressure between the two gold plates was controlled by applying a pneumatic pressure to the bottom plate. The voltage was measured between the top gold coated copper plate and a spring loaded gold pin in the middle of the bottom gold coated copper plate using a Fluke 76 True RMS multimeter. From this voltage, the ICR was calculated by Ohms law.

Surface analysis methods.—Scanning Electron Microscopy (SEM, Hitachi S-3400N), Field Emission Gun Scanning Electron Microscopy (FEGSEM, Zeiss Ultra), Auger Electron Spectroscopy (AES, JEOL JAMP-9500) and X-ray Photoelectron Spectroscopy (XPS, Axis Ultra^{DLD}) were used to characterize the coated plates both before and after polarization.

Results and Discussion

Parameter variations.—A set of test parameters were defined as baseline polarization conditions during this study (Table I). Temperature, pH, cell potential and test duration were altered in order to study the effect this would have on the current and ICR. Note that only one parameter was altered at a time. Alteration of working electrode potential and duration of polarization were studied in depth, as these parameters proved to have the most impact on both polarization currents and ICR.

At high potentials, the measured cell current arose from both degradation of the material and oxygen evolution. Weight loss was measured for each sample with a digital scale, but neither of the Ta-ITO coated titanium samples showed significant weight loss during polarization. It was thus assumed that most of the current produced during polarization of the Ta-ITO coated titanium samples was caused by oxygen evolution. The ICR results were therefore assumed to provide more accurate information about the alteration in the Ta-ITO coating during polarization. The ICR values obtained at 140 N cm^{-2} after polarization of all the samples in the parameter study are displayed in Fig. 2. The black bar in the chart shows the ICR of an unpolarized Ta-ITO coated titanium plate. Polarization of non-coated gold, platinum and titanium are also included in the figure as references.

For bipolar plates in fuel cells, the US Department of Energy (DoE)[47] has set targets including current densities below 1 μA cm^{-2} and ICR values below 10 mΩ cm^2. Even though these targets do not apply for BPPs in PEMWE, they provide an indication of the order of magnitude acceptable for current and resistance. The interfacial contact resistance measured before polarization of the Ta-ITO coated titanium plate was 10 mΩ cm^2, and after polarization at baseline conditions it was 15 mΩ cm^2. These values are both close to DoE's target for ICR. As can be seen from Fig. 2, the highest ICR value obtained was measured on the Ta-ITO coated titanium that had been polarized at 2.6 V_{RHE} (503 mΩ cm^2). The lowest value for the Ta-ITO coated samples after polarization was obtained from the sample that had been polarized at room temperature. This was to be expected, as temperature is known to accelerate corrosion processes on the surface, resulting in alteration of the oxide layer conductivity.

As expected, both gold and platinum showed lower ICR after polarization than any of the other samples in this study. Neither of these materials are known to corrode to any significance when polarized in the anodic direction. When comparing non-coated titanium to the Ta-ITO coated titanium, it is evident that the non-coated titanium experienced a higher increase in ICR after the baseline test. This is particularly interesting considering the fact that titanium is most commonly used as BPP in PEMWE today.

Zhang et al.[15] measured ICR on Ti-Ag-N coated titanium for use in regenerative fuel cells. After polarization at 2.0 V_{SCE} in 0.5 M H_2SO_4 + 2 ppm F^-, the ICR of the Ti-Ag-N coated titanium was reported to be between 2.3 and 7.0 mΩ cm^2. Zhang et al.[14] coated titanium with Ti-Ag and found the ICR to increase from 4.1 mΩ cm^2 to 22.2 mΩ cm^2 after polarization at 2.0 V_{NHE} in 0.5 M H_2SO_4 + 5 ppm F^-. These numbers are all in the same order of magnitude as the ICR obtained from the Ta-ITO coatings.

Figure 3 shows pictures and SEM images of Ta-ITO coated plates both before and after polarization. The circular mark on the polarized samples were from the O-ring in the working electrode setup, and only the area inside this circle was exposed to the electrolyte. The SEM images in the middle column were obtained at a magnification of 1000x, and the images at the right were obtained at a magnification of 10 000x. The images in the same rows are from the same sample. Figure 3A shows the unpolarized sample, 3B shows the sample that had been polarized at baseline conditions, 3 C

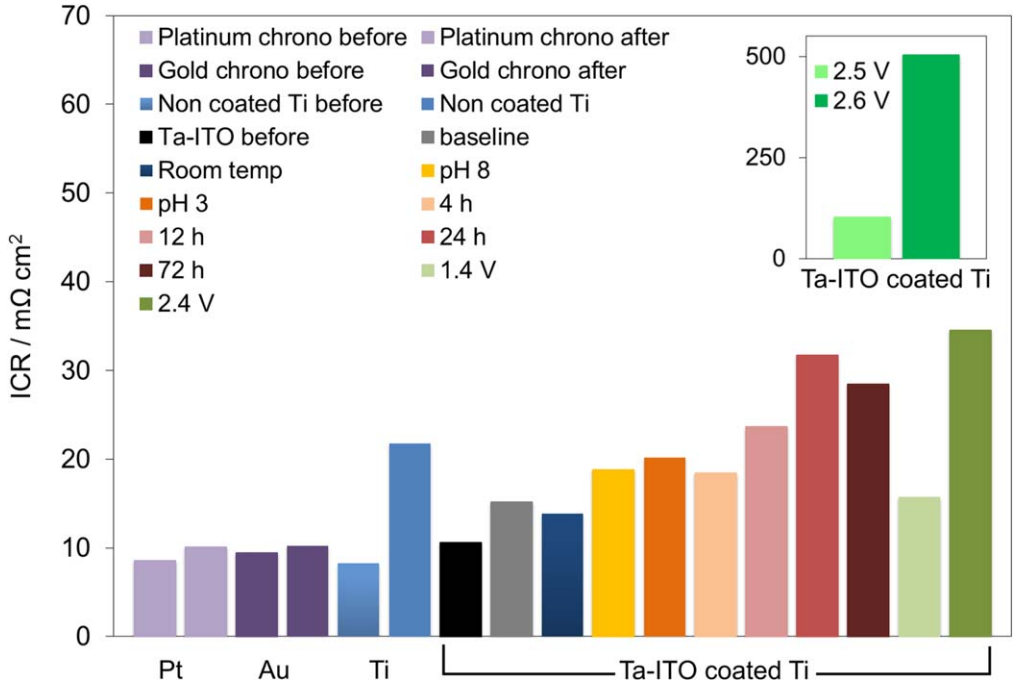

Figure 2. ICR values obtained from the plates used in all the potentiostatic tests in this study (Table I) before and after polarization at 2.0 V_{RHE} for 1 h. A compaction pressure of 140 Ncm^{-2} was used for all the ICR measurements, and when the material is not specified, it is Ta-ITO coated titanium.

shows the sample that had been polarized for 24 h and Fig. 3D shows the sample that had been polarized at 2.6 V_{RHE}.

These samples were chosen as they showed great variation in ICR values obtained after polarization. From both the pictures and SEM images it is evident that the surfaces of the samples are very similar. The SEM images show a similar surface structure on all four samples. Assessment of the pictures and SEM images separately gave no indication of any corrosion or surface alterations after polarization.

Time variations.—Figures 4 and 5 show results obtained from the Ta-ITO coated titanium samples that had been polarized for various durations of time. One hour tests can be used for screening of materials and coatings, but as electrolyzers should operate for much longer periods of time, it is important to extend such tests to see how the current and ICR develop over time. Figure 4 shows how the current density develops over time for a series of Ta-ITO coated titanium samples. The current densities are of similar magnitude and are in general quite low, with a similar continuous and slow decline with time. As mentioned earlier, the current on most materials at 2.0 V_{RHE} in acidic aqueous electrolytes, is greatly influenced by oxygen evolution at the surface. Furthermore, none of the samples in this study showed significant weight loss during polarization, and it was thus assumed that most of the current observed originated from other surface reactions than corrosion. As mentioned, nitrogen bubbling was not used during the long term polarizations, to avoid evaporation of electrolyte. The presence of oxygen was probably higher at the beginning of the long term tests (12 h, 24 h, and 72 h).

Figure 5 shows the development of ICR with time, and it is evident that the ICR stabilizes somewhere between 12 and 24 h. This

Table I. Polarization parameters used for the potentiostatic and potentiodynamic polarizations in this study.

Name	Substrate	Coating	Temperature [°C]	pH	Potential [V_{RHE}]	Duration/sweep rate
Baseline	Ti	Ta + ITO	60	5.5	2.0	3600 s
Ta-ITO sweep	Ti	Ta + ITO	60	5.5	0–2.0	1 mV s^{-1}
1.4 V	Ti	Ta + ITO	60	5.5	1.4	3600 s
2.4 V	Ti	Ta + ITO	60	5.5	2.4	3600 s
2.5 V	Ti	Ta + ITO	60	5.5	2.5	3600 s
2.6 V	Ti	Ta + ITO	60	5.5	2.6	3600 s
pH 3	Ti	Ta + ITO	60	3	2.0	3600 s
pH 8	Ti	Ta + ITO	60	8	2.0	3600 s
Room temp	Ti	Ta + ITO	20	5.5	2.0	3600 s
4 h	Ti	Ta + ITO	60	5.5	2.0	4 h
12 h	Ti	Ta + ITO	60	5.5	2.0	12 h
24 h	Ti	Ta + ITO	60	5.5	2.0	24 h
72 h	Ti	Ta + ITO	60	5.5	2.0	72 h
Non coated Ti	Ti	None	60	5.5	2.0	3600 s
Gold chrono	Au	None	60	5.5	2.0	3600 s
Gold sweep	Au	None	60	5.5	0–2.0	1 mV s^{-1}
Platinum chrono	Pt	None	60	5.5	2.0	3600 s
Platinum sweep	Pt	None	60	5.5	0–2.0	1 mV s^{-1}

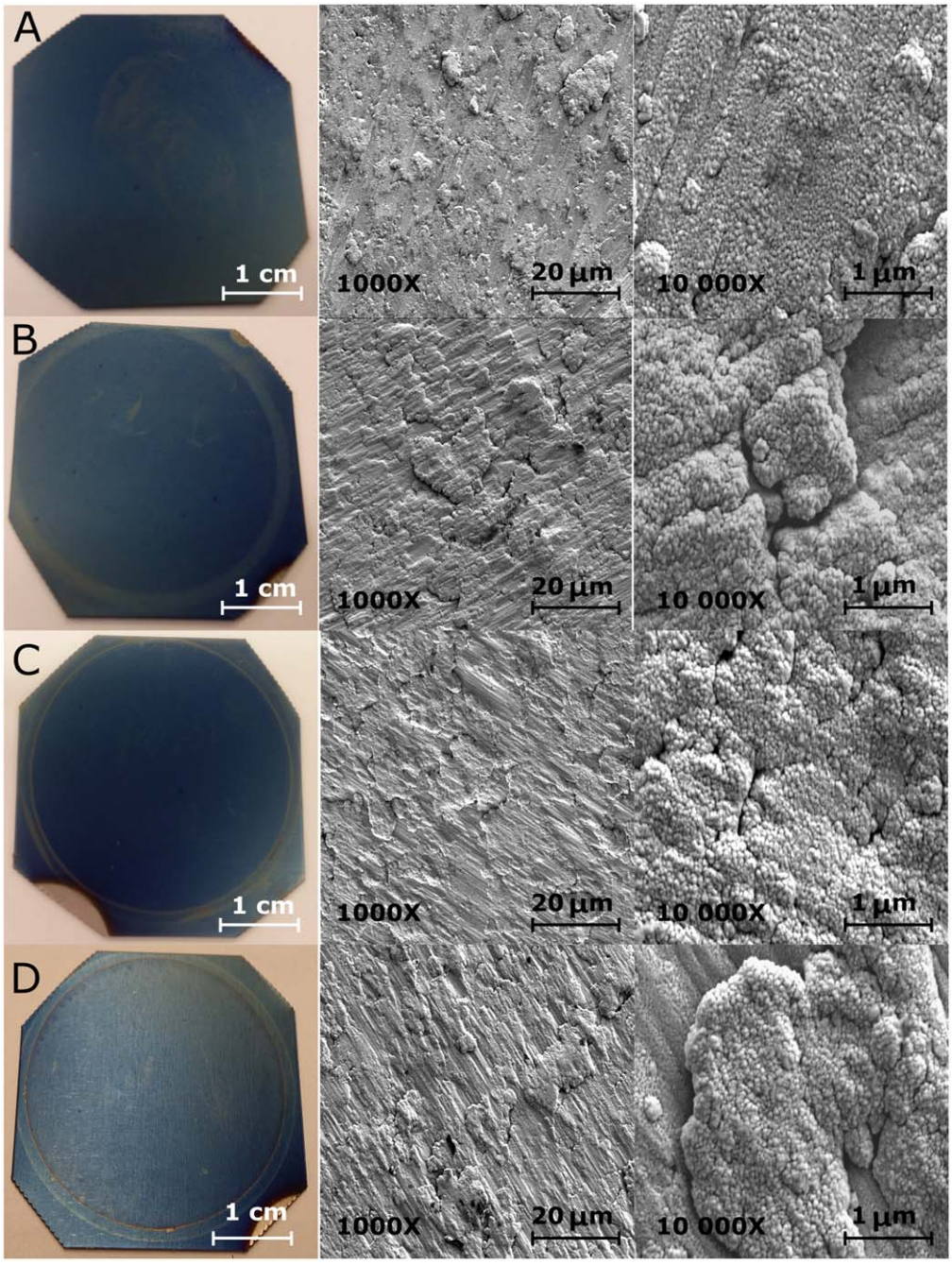

Figure 3. Pictures and SEM images of Ta-ITO coated Ti obtained (A) Before polarization, (B) After polarization at baseline conditions, (C) After polarization for 24 h and (D) After polarization at 2.6 V_{RHE}.

is interesting, as this indicates that the ICR will remain stable over time. The small decrease from 24 to 72 h is most likely an indication of the experimental spread in such measurements. The error bars only reflect the experimental uncertainty in the ICR measuring device. It is important to note that the ICR does increase from 15 mΩ cm^2 after 1 h to 32 mΩ cm^2 after 24 h, but the absolute values are still small compared to the highest ICR value (503 mΩ cm^2) obtained in this study (Fig. 2).

Figure 5B shows how the ICR developed over time for non-coated titanium when polarized at 2.0 V_{RHE}.[46] The ICR for non-coated titanium increased continuously with time, and was still increasing after 122 h of polarization at 2.0 V_{SHE}. This is not the same trend seen for the Ta-ITO coated samples, where the current stabilized around 24 h. In addition, the absolute values of the ICR in Fig. 4.8 are higher than the values in Fig. 5. These results show a very promising trend for the Ta-ITO coating, and might be a better option than the non-coated Ti used today.

Potential variations.—Figure 6 shows the contact resistances obtained after polarization of the Ta-ITO coated titanium plates at various potentials. The Ta-ITO plates that had been polarized at 1.4 V_{RHE} and 2.0 V_{RHE} showed very similar resistances, while the ICR started to increase when the potential was increased to 2.4 V_{RHE}. As displayed in Fig. 6, the slope of the curve changes drastically after 2.4 V_{RHE}. When the potential is changed from 2.4 V_{RHE} to 2.5 V_{RHE}, the ICR value was tripled. Between 2.5 V_{RHE} and 2.6 V_{RHE} the ICR increased by a factor of 5 (Fig. 2). It is thus evident that even higher potentials cause significant changes in the surface properties of the coated samples, leading to significantly reduced electrical conductivity. This change was not evident in the pictures and images

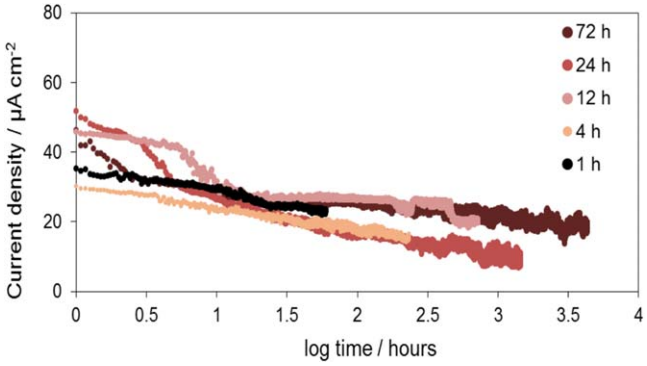

Figure 4. Current development over time for the Ta-ITO coated titanium when polarized potentiostatically at 2.0 V_{RHE}.

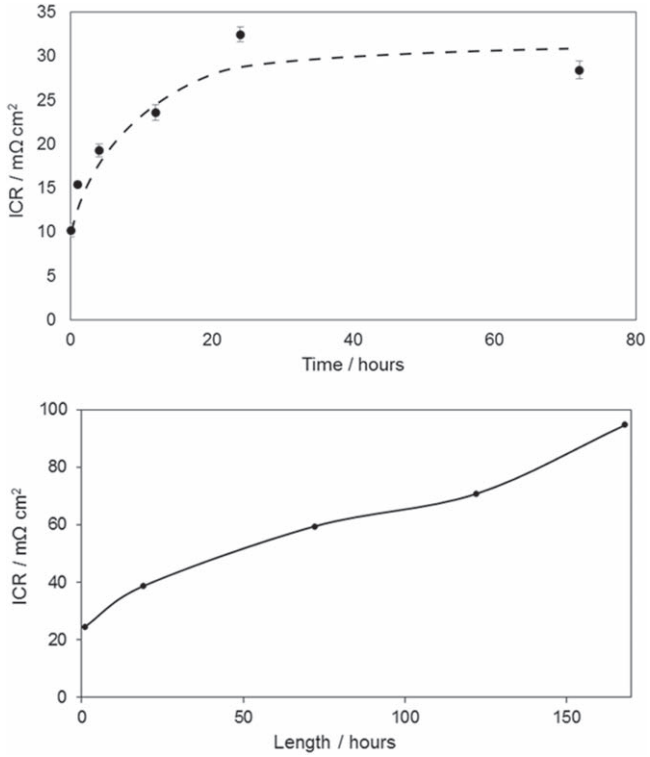

Figure 5. (A) Development of ICR with time for the Ta-ITO coated titanium when polarized potentiostatically at 2.0 V_{RHE}. (B) ICR at 140 N cm^{-2} after potentiostatic polarization of titanium at 2.0 V_{SHE} over different time spans.[46]

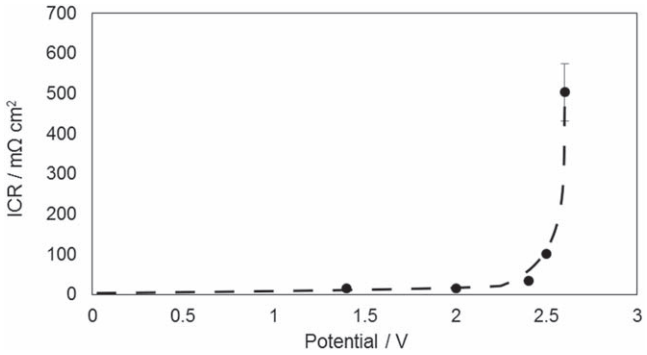

Figure 6. ICR values obtained from the Ta-ITO coated titanium plates after polarization at different potentials. All the ICR values were obtained at a compaction pressure of 140 N cm^{-2}.

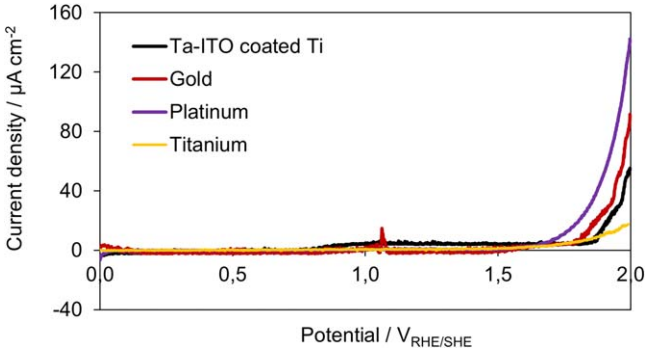

Figure 7. Potentiodynamic polarization curves for gold, platinum and Ta-ITO coated Ti (all vs RHE) compared to the results previously obtained by Lædre et al. for uncoated titanium at baseline conditions (vs SHE).[48]

Table II. ICR values at 140 N cm^{-2} obtained from platinum-, gold-, and Ta-ITO coated titanium before and after potentiodynamic polarization at 2 V_{RHE}. Results previously obtained by Lædre et al. for uncoated titanium is included for comparison.[48]

	ICR at 140 N cm^{-2} [mΩ cm^2]	
Material	Before Polarization	After Polarization
Platinum	9	9
Gold	10	10
Ta-ITO coated titanium	10	16
Non-coated titanium[a)]	8	25

a) Found by Lædre et al. in previous study.[48]

presented in Fig. 3, where the 2.0 V_{RHE} and 2.6 V_{RHE} samples were compared.

Potentiodynamic polarization.—In addition to the potentiostatic polarizations in this study, potentiodynamic polarization curves were obtained for gold, platinum and Ta-ITO coated titanium, and similar results from Lædre et al.[48] have been included for uncoated Titanium. The results from the polarization are presented in Fig. 7, while the ICR obtained before and after each sweep is presented in Table II. The majority of the currents produced during the polarizations of all four materials were most likely caused by oxygen evolution. The onset of current increase is a bit different for the four materials, but for all but titanium the current increases drastically after 1.7 V. As no significant weight loss was observed for the Ta-ITO coated sample, it was assumed that it did not corrode significantly. The observed difference between the linear sweeps could be attributed to the variations of the electrochemical nature for oxygen evolution at the surface of the four materials. The ICR did not change during polarization for gold or platinum, and the change for the Ta-ITO coated titanium was lower than for bare titanium. It was also similar to the ICR obtained after the potentiostatic polarization. For Titanium the

AES and XPS characterization.—Auger electron spectroscopy was used in order to understand why such a substantial increase in ICR was observed for the samples that had been polarized at 2.5 V_{RHE} and 2.6 V_{RHE} for one hour. AES provided relative amounts of each component (tantalum, indium, oxygen and tin) as a function of depth in four different Ta-ITO coated titanium samples. The 2.5 V_{RHE} plate and the 2.6 V_{RHE} plate were chosen as they showed the highest ICR values after polarization of all the tested plates, with 102 mΩ cm^2 and 503 mΩ cm^2, respectively. An unpolarized plate and the baseline sample were also analyzed by AES, as they had shown relatively low ICR values compared to the two other samples.

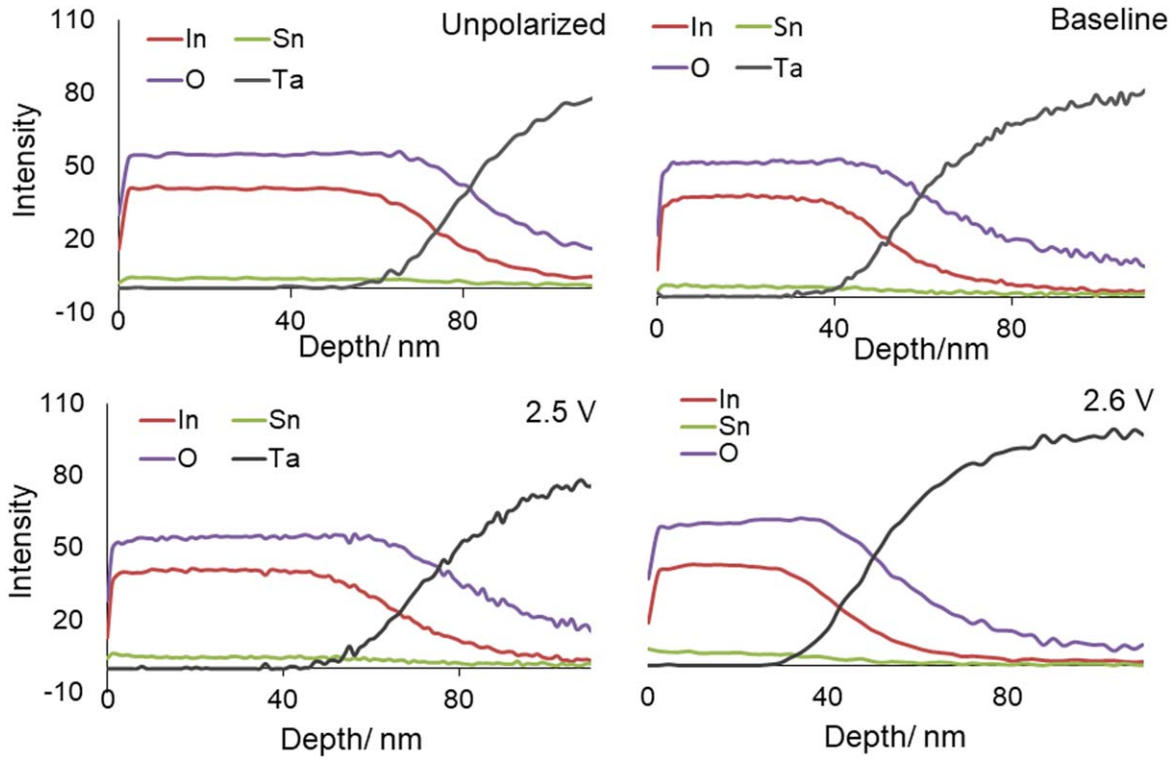

Figure 8. AES analysis performed on four Ta-ITO plates, one unpolarized and three polarized as described in Table I.

The results are presented in Fig. 8, where the oxide thickness can be estimated based on the oxygen intensity with depth. From this, it looks like the unpolarized sample and the 2.5 V_{RHE} sample had a thicker oxide than the other two, and that the 2.6 V_{RHE} sample obtained the thinnest oxide layer. In addition, no significant change in composition was observed for either of the samples. Based on the ICR measurements, these findings were surprising as one would assume that the oxide layer on the sample surfaces possessed the same properties with respect to conductivity, and that a thicker oxide would be expected to result in a higher rather than lower ICR. There is not a clear trend when the AES and ICR results are compared for the four samples below, and it became evident that further analysis was necessary to understand the increase in ICR for the 2.5 V_{RHE} and 2.6 V_{RHE} samples.

As the AES analysis was inconclusive, XPS was performed on the same four samples. The results are shown in Table III and Fig. 9. Table III shows the composition of the coatings and the relationship between indium and tin. The ratio between oxygen content and (indium + tin) in the 2.5 V_{RHE} and 2.6 V_{RHE} samples are higher than for the unpolarized and baseline samples. This means that there is more oxygen compared to metal in the upmost part of the samples polarized at higher voltages, which could explain the higher ICR values obtained from the 2.5 V_{RHE} and 2.6 V_{RHE} samples. The XPS analysis also showed a decrease in the indium/tin ratio from top to bottom in the table. The unpolarized sample has close to 9 times more indium than tin, the baseline sample has 6.15, the 2.5 V_{RHE} sample has 3.83 and the 2.6 V_{RHE} sample has only 2.69 times more indium than tin.

Table III. Composition of oxygen, carbon, indium and tin in the samples analyzed by XPS. The oxygen/metal ratio and indium/tin ratio is also included.

Sample	Core level	Composition (atom %)	O/(In + Sn) ratio	In/Sn ratio
Unpolarized	In 3d	25.0	1.42	8.88
	O 1 s	39.6		
	C 1 s	32.9		
	Sn 3d	2.8		
Baseline	In 3d	14.6	1.82	6.15
	O 1 s	31.0		
	C 1 s	52.0		
	Sn 3d	2.5		
2.5 V	In 3d	13.1	1.93	3.83
	O 1 s	31.9		
	C 1 s	51.6		
	Sn 3d	3.4		
2.6 V	In 3d	10.6	2.10	2.69
	O 1 s	30.5		
	C 1 s	55.0		
	Sn 3d	3.9		

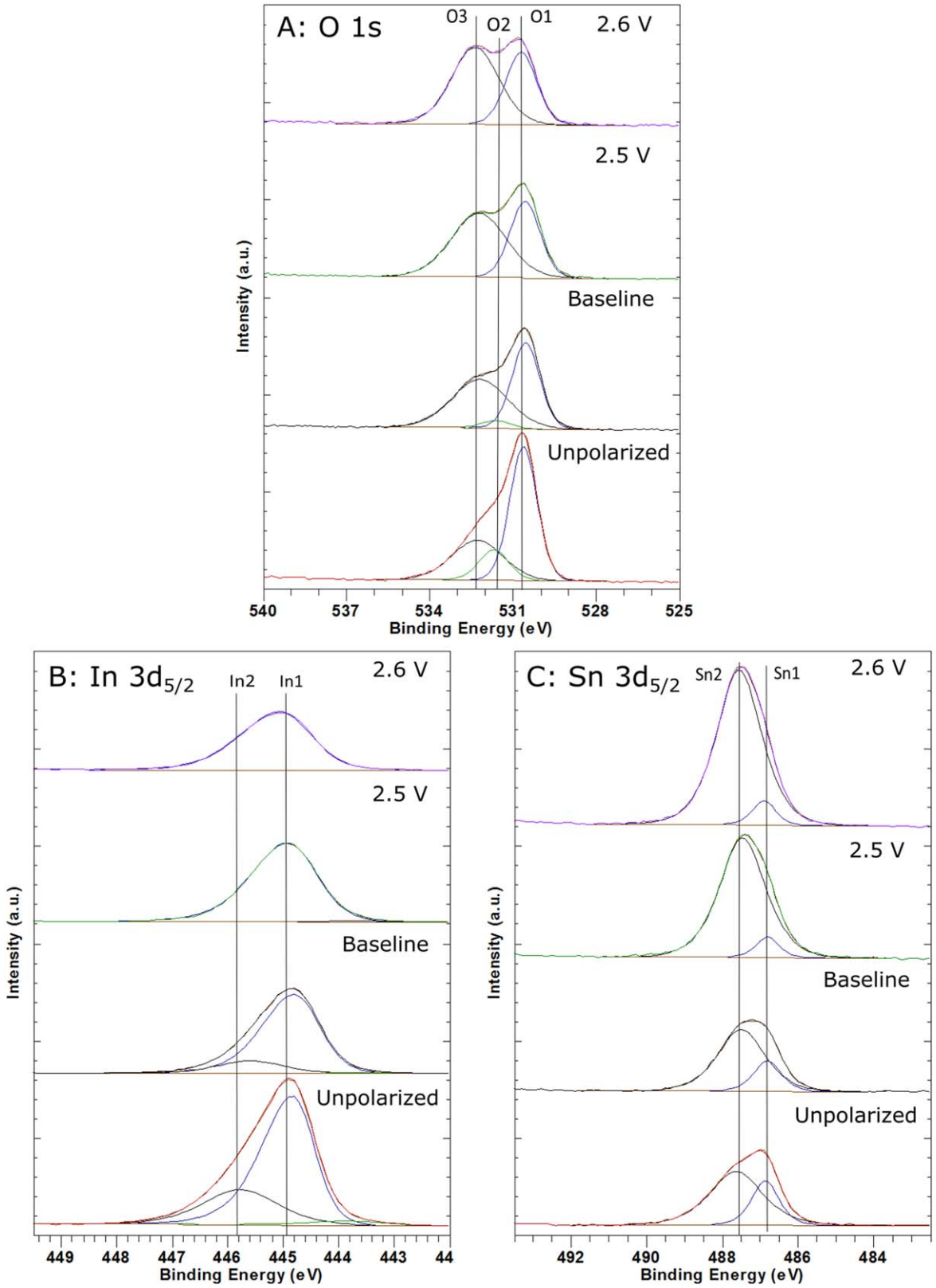

Figure 9. XPS spectrums obtained from four of the samples in this study (Table I) showing binding energies of oxygen, indium and tin.

The trend in the In/Sn ratio is opposite of the ICR values in Table II, indicating that a low indium/tin ratio correlated with a high ICR value. The reason for the ratio decrease in the 2.5 V_{RHE} and 2.6 V_{RHE} samples is due to an enrichment of Sn and a removal of In from surface of the samples. Indium could dissolve into the electrolyte due to selective dissolution from e.g. selective corrosion, and this would also explain in part why the AES measurements showed a decrease in ITO thickness. Thirumoorthi and Prakash[49] found the resistivity of ITO to decrease with increasing Sn weight percent, from 0.9 mΩ-cm with 0 wt % Sn to 0.4 mΩ-cm at 30 wt %

Sn. However, this is a lower decrease compared to the increase in ICR found in this study, and other effects are thus assumed to be responsible for the observed increase in the ICR values for the 2.5 V_{RHE} and 2.6 V_{RHE} samples.

Figure 9 shows the XPS spectrums of oxygen (O 1 s), indium (In $3d_{5/2}$) and tin (Sn $3d_{5/2}$) obtained from the unpolarized, baseline, 2.5 V_{RHE} and 2.6 V_{RHE} samples. The peaks are each related to the binding energy between the various elements on the surface of the samples. Three peaks were observed for oxygen in in this analysis (Fig. 9A). O1 and O3 are present in all four samples, and they both increase in height from bottom to top in Fig. 9A. The O1 peak is associated with the oxygen found in the ITO layer as it was deposited on the titanium surface.[50] The O3 peak is associated with hydroxides, indicating that the amount of hydroxides on the surface of the samples increase from bottom to top.[50–52] The O2 peak is only present in the unpolarized and baseline samples. This peak is associated with oxygen in a configuration where it is adjacent to oxygen vacancies in the structure.[53] This indicates that the number of oxygen vacancies on the surfaces of the 2.5 V_{RHE} and 2.6 V_{RHE} samples were lower than the other two samples. Oxygen vacancies are known for increasing the electrical conductivity of a material,[34] and for ITO oxygen vacancies are associated with increased conductivity as this will add two electrons to the conduction band and thus increase the free carrier concentration. The high ICR obtained from the 2.5 V_{RHE} and 2.6 V_{RHE} could thus be partially caused by the lower number of oxygen vacancies.

Two peaks can be seen for indium in the spectrums shown in Fig. 9B. In1 is found in the spectra obtained from all four samples, but In2 is only found in the spectras from the unpolarized and baseline samples. In 1 is associated with In^{3+} in In_2O_3 like species.[53] The In1 peak lost its asymmetry from bottom to top in Fig. 5.9B, which indicates that the metallic character of indium is weakened from bottom to top. Smaller degrees of asymmetry could result in lower conductivity,[54,55] which can explain the higher ICR observed for the 2.5 V_{RHE} and 2.6 V_{RHE} samples. The In2 peak is associated with indium in e.g. In-OH and In-OOH species,[50,53] which coincides well with the O2 peak.

The spectra obtained showed two tin peaks (Fig. 9C), Sn1 and Sn2. The first one is associated with Sn in SnO_2-like species.[52,53] The Sn2 peak can be associated with different compounds, but in this case, it corresponded well with the with the O3 peak, indicating that it is from a tin hydroxide.

When looking at all the XPS spectra combined, it is clear that there was an increase in hydroxides on the surface of the 2.5 V_{RHE} and the 2.6 V_{RHE} samples compared to the other two, which increases with polarization potential. In addition, there is a decrease in oxygen adjacent to oxygen vacancies for the same two samples, as well as a decrease in metallic character for indium. All of these factors explain why the ICR for the samples were so high compared to all the other Ta-ITO coated titanium samples in this study.

Conclusions

The Ta-ITO bi-layer coating was successfully applied to a titanium surface by use of magnetron sputtering. The coating was polarized under various conditions, resulting in very low corrosion currents. As the weight loss measured for all the samples were lower than the error of the measurements, it was assumed that the current produced during polarization was caused by oxygen evolution. Pictures and SEM images obtained before and after polarization showed no changes on the coated surfaces, even after polarization at 2.6 V_{RHE}. Alteration of pH and temperature proved to have little or no effect on the interfacial contact resistance. Potentials above 2.0 V_{RHE} and polarization longer than 1 h resulted in higher ICR value. The Ta-ITO coated titanium plate that had been polarized at 2.6 V_{RHE} showed an ICR value of 503 mΩ cm^2 compared to 15 mΩ cm^2 for the sample polarized at 2.0 V_{RHE}.

XPS analysis showed that there was an increase in hydroxides on the surface of the 2.5 V_{RHE} and 2.6 V_{RHE} samples compared to the unpolarized and baseline samples, and that the increase was related to higher polarization potentials. For the same two samples, there was a decrease in oxygen vacancies and a decrease in metallic character for indium. The oxygen to metal ratio on the Ta-ITO coated samples surfaces was found to increase on the 2.5 V_{RHE} and 2.6 V_{RHE} samples, and the indium to tin ratio was found to decrease, likely caused by selective dissolution of indium. Combined, all of these factors could explain why the ICR values for the 2.5 V_{RHE} and 2.6 V_{RHE} were so much higher than for all the other samples in this study. However, polarization at such high potentials is not realistic for BPPs in PEMWE. When the Ta-ITO coated titanium plates were polarized at 2.0 V_{RHE} for more than one day, the ICR stabilized at about 30 mΩ cm^2. This means that Ta-ITO films are very promising as BPP material in the harsh PEMWE environment.

Acknowledgments

The late Dr Ole Edvard Kongstein is greatly acknowledged for his contributions to this work. Ingeborg Svenum and John Walmsley also contributed with XPS and AES analysis, respectively. The Norwegian University of Science and Technology is acknowledged for the award of a scholarship. The work was also funded by SINTEF Industry through the COATELY project.

ORCID

Sigrid Lædre https://orcid.org/0000-0002-4234-2979
Lucia Mendizabal https://orcid.org/0000-0002-5886-9724
Anders Oedegaard https://orcid.org/0000-0002-9277-0170

References

1. C.-J. Winter, *Int. J. Hydrogen Energy*, **34**, S1 (2009).
2. A. Ursua, L. M. Gandia, and P. Sanchis, *Proc. IEEE*, **100**, 410 (2012).
3. P. Millet, A. Ranjbari, F. De Guglielmo, S. A. Grigoriev, and F. Auprêtre, *Int. J. Hydrogen Energy*, **37**, 17478 (2012).
4. M. Carmo, D. L. Fritz, J. Mergel, and D. Stolten, *Int. J. Hydrogen Energy*, **38**, 4901 (2013).
5. F. Barbir, *Sol. Energy*, **78**, 661 (2005).
6. J.-T. Wang, W.-W. Wang, C. Wang, and Z.-Q. Mao, *Int. J. Hydrogen Energy*, **37**, 12069 (2012).
7. S. Shiva Kumar and V. Himabindu, *Materials Science for Energy Technologies*, **2**, 442 (2019).
8. P. Millet, F. Andolfatto, and R. Durand, *Int. J. Hydrogen Energy*, **21**, 87 (1996).
9. S. A. Grigoriev, P. Millet, S. A. Volobuev, and V. N. Fateev, *Int. J. Hydrogen Energy*, **34**, 4968 (2009).
10. K. E. Ayers, E. B. Anderson, C. Capuano, B. Carter, L. Dalton, G. Hanlon, J. Manco, and M. Niedzwiecki, *ECS Trans.*, **33**, 3 (2010).
11. H.-Y. Jung, S.-Y. Huang, P. Ganesan, and B. N. Popov, *J. Power Sources*, **194**, 972 (2009).
12. H.-Y. Jung, S.-Y. Huang, and B. N. Popov, *J. Power Sources*, **195**, 1950 (2010).
13. M.-T. Lin, C.-H. Wan, and W. Wu, *Thin Solid Films*, **544**, 162 (2013).
14. H. Zhang, M. Hou, G. Lin, Z. Han, Y. Fu, S. Sun, Z. Shao, and B. Yi, *Int. J. Hydrogen Energy*, **36**, 5695 (2011).
15. M. Zhang, L. Hu, G. Lin, and Z. Shao, *J. Power Sources*, **198**, 196 (2012).
16. A. V. Nikiforov, I. M. Petrushina, E. Christensen, A. L. Tomás-García, and N. J. Bjerrum, *Int. J. Hydrogen Energy*, **36**, 111 (2011).
17. M. Langemann, D. L. Fritz, M. Müller, and D. Stolten, *Int. J. Hydrogen Energy*, **40**, 11385 (2015).
18. A. S. Gago et al., *J. Power Sources*, **307**, 815 (2016).
19. G. Yang, J. Mo, Z. Kang, F. A. List, J. B. Green, S. S. Babu, and F.-Y. Zhang, *Int. J. Hydrogen Energy*, **42**, 14734 (2017).
20. R. S. Hansen, S. E. Johnsen, H. J. Fell, and E. Rasten, *Patent: Use of austenitic stainless steel as construction material in a device or structural component which is exposed to an oxygen and/or hydrogen and/or hydrofluoric acid environment*, US20060141333A1 (2010), Hydrogen Technologies AS Hydrogen Tech AS, United States of America.
21. N. Rojas, M. Sánchez-Molina, G. Sevilla, E. Amores, E. Almandoz, J. Esparza, M. R. Cruz Vivas, and C. Colominas, *Int. J. Hydrogen Energy*, **46**, 25929 (2021).
22. A. Cacucci, S. Loffredo, V. Potin, L. Imhoff, and N. Martin, *Surf. Coat. Technol.*, **227**, 38 (2013).
23. S. V. Jagadeesh Chandra, C.-J. Choi, S. Uthanna, and G. Mohan Rao, *Mater. Sci. Semicond. Process.*, **13**, 245 (2010).
24. Y.-Y. Chang, H.-L. Huang, H.-J. Chen, C.-H. Lai, and C.-Y. Wen, *Surf. Coat. Technol.*, **259Part B**, 193 (2014).
25. C. J. Frandsen, K. S. Brammer, K. Noh, G. Johnston, and S. Jin, *Mater. Sci. Eng. C*, **37**, 332 (2014).
26. K. J. Kumar, N. R. C. Raju, and A. Subrahmanyam, *Surface and Coatings Technology,*, **205Supplement 2**, S261 (2011).
27. F. Meng, Z. Li, and X. Liu, *Surf. Coat. Technol.*, **229**, 205 (2013).

28. B. Rahmati, A. A. D. Sarhan, E. Zalnezhad, Z. Kamiab, A. Dabbagh, D. Choudhury, and W. A. B. W. Abas, *Ceram. Int.*, **42**, 466 (2016).
29. K. Tajima, Y. Yamada, S. Bao, M. Okada, and K. Yoshimura, *Solid State Ionics*, **180**, 654 (2009).
30. J. Black, *Clin. Mater.*, **16**, 167 (1994).
31. L. Wang, L. Li, H. Liu, S. Wang, H. Fang, H. Gao, K. Gao, Y. Zhang, J. Sun, and J. Yan, *J. Power Sources*, **399**, 343 (2018).
32. M. Alishahi, F. Mahboubi, S. M. Mousavi Khoie, M. Aparicio, R. Hübner, F. Soldera, and R. Gago, *J. Power Sources*, **322**, 1 (2016).
33. S.-Y. Lien, *Thin Solid Films*, **518**, S10 (2010).
34. H. Kim, C. M. Gilmore, A. Piqué, J. S. Horwitz, H. Mattoussi, H. Murata, Z. H. Kafafi, and D. B. Chrisey, *J. Appl. Phys.*, **86**, 6451 (1999).
35. X. D. Liu, E. Y. Jiang, and D. X. Zhang, *J. Appl. Phys.*, **104**, 073711 (2008).
36. G. Korotcenkov, V. Brinzari, A. Cerneavschi, M. Ivanov, V. Golovanov, A. Cornet, J. Morante, A. Cabot, and J. Arbiol, *Thin Solid Films*, **460**, 315 (2004).
37. T. Maruyama and K. Fukui, *Thin Solid Films*, **203**, 297 (1991).
38. K. Daoudi, B. Canut, M. G. Blanchin, C. S. Sandu, V. S. Teodorescu, and J. A. Roger, *Thin Solid Films*, **445**, 20 (2003).
39. S. H. Cho, J. H. Park, S. C. Lee, W. S. Cho, J. H. Lee, H. H. Yon, and P. K. Song, *J. Phys. Chem. Solids*, **69**, 1334 (2008).
40. L. Kerkache, A. Layadi, E. Dogheche, and D. Rémiens, *J. Phys. D: Appl. Phys.*, **39**, 184 (2006).
41. L. Juhn-Jong and L. Zhi-Qing, *J. Phys. Condens. Matter*, **26**, 343201 (2014).
42. O. Bierwagen, *Semicond. Sci. Technol.*, **30**, 024001 (2015).
43. S. J. Nadel, P. Greene, J. Rietzel, and J. Strümpfel, *Thin Solid Films*, **442**, 11 (2003).
44. K. Sarakinos, J. Alami, and S. Konstantinidis, *Surf. Coat. Technol.*, **204**, 1661 (2010).
45. J. Lin, J. J. Moore, W. D. Sproul, S. L. Lee, and J. Wang, *IEEE Trans. Plasma Sci.*, **38**, 3071 (2010).
46. S. Lædre, O. E. Kongstein, A. Oedegaard, H. Karoliussen, and F. Seland, *Int. J. Hydrogen Energy*, **42**, 2713 (2017).
47. U.S. Department of Energy, *Fuel Cell Technologies Office Multi-Year Research, Development, and Demonstration Plan*, p. 29 (2012).
48. V. Mishra, F. Yang, and R. Pitchumani, *J. Fuel Cell Sci. Technol.*, **1**, 2 (2004).
49. M. Thirumoorthi and J. T. J. Prakash, *Journal of Asian Ceramic Societies*, **4**, 124 (2016).
50. C. Nunes de Carvalho, A. M. Botelho do Rego, A. Amaral, P. Brogueira, and G. Lavareda, *Surf. Coat. Technol.*, **124**, 70 (2000).
51. J. Zhu, J. Yang, Z.-F. Bian, J. Ren, Y.-M. Liu, Y. Cao, H.-X. Li, H.-Y. He, and K.-N. Fan, *Appl. Catalysis B*, **76**, 82 (2007).
52. F. Montilla, E. Morallón, A. De Battisti, S. Barison, S. Daolio, and J. L. Vázquez, *J. Phys. Chem. B*, **108**, 15976 (2004).
53. A. Thøgersen, M. Rein, E. Monakhov, J. Mayandi, and S. Diplas, *J. Appl. Phys.*, **109**, 113532 (2011).
54. Y. Gassenbauer and A. Klein, *J. Phys. Chem. B*, **110**, 4793 (2006).
55. Y. Gassenbauer, A. Wachau, and A. Klein, *Phys. Chem. Chem. Phys.*, **11**, 3049 (2009).